Plasma Pharmacokinetics of N-Acetylgalactosamine-Conjugated Small-Interfering Ribonucleic Acids (GalNAc-Conjugated siRNAs)

LEADING ARTICLE

Plasma Pharmacokinetics of N-Acetylgalactosamine-Conjugated Small-Interfering Ribonucleic Acids (GalNAc-Conjugated siRNAs)

Sebastian Sten[1] · Tim Cardilin[2] · Madeleine Antonsson[1] · Peter Gennemark[1,3]

Abstract

Small-interfering ribonucleic acids (siRNAs) with N-acetylgalactosamine (GalNAc) conjugation for improved liver uptake represent an emerging class of drugs that modulate liver-expressed therapeutic targets. The pharmacokinetics of GalNAc-siRNAs are characterized by a rapid distribution from plasma to tissue (hours) and a long terminal plasma half-life, analyzed in the form of the antisense strand, driven by redistribution from tissue (weeks). Understanding how clinical pharmacokinetics relate to the dose and type of siRNA chemical stabilizing method used is critical, e.g., to design studies, to investigate safety windows, and to predict the pharmacokinetics of new preclinical assets. To this end, we collected and analyzed pharmacokinetic data from the literature regarding nine GalNAc-siRNAs. Based on this analysis, we showed that the clinical plasma pharmacokinetics of GalNAc-siRNAs are approximately dose proportional and similar between chemical stabilizing methods. This holds for both the area under the concentration-time curve (AUC) and the maximum plasma concentration (C_{max}). Corresponding rat and monkey pharmacokinetic data for a subset of the nine GalNAc-siRNAs show dose-proportional C_{max}, supra-dose-proportional AUC, and similar pharmacokinetics between chemical stabilizing methods. Together, the animal and human pharmacokinetic data indicate that plasma clearance divided by bioavailability follows allometric principles and scales between species with an exponent of 0.75. Finally, the clinical plasma concentration-time profiles can be empirically described by standard one-compartment kinetics with first-order absorption up to 24 h after subcutaneous dosing, and by three-compartment kinetics with first-order absorption in general. To describe the system more mechanistically, we report a corrected and unambiguously defined version of a previously published physiologically based pharmacokinetic model.

1 Introduction

Small-interfering ribonucleic acids (siRNAs) with N-acetylgalactosamine (GalNAc) conjugation for improved liver uptake represents an emerging class of drugs to treat various liver diseases [1]. Several GalNAc-siRNAs have

---

Sebastian Sten and Tim Cardilin contributed equally to this work.

✉ Peter Gennemark
  peter.gennemark@astrazeneca.com

1 Drug Metabolism and Pharmacokinetics, Research and Early Development, Cardiovascular, Renal and Metabolism (CVRM), BioPharmaceuticals R&D, AstraZeneca, Gothenburg, Sweden

2 Fraunhofer-Chalmers Research Centre for Industrial Mathematics, Chalmers Science Park, 41288 Gothenburg, Sweden

3 Department of Biomedical Engineering, Linköping University, Linköping, Sweden

Key Points

Clinical plasma pharmacokinetic data for nine N-acetylgalactosamine-conjugated small-interfering RNAs (GalNAc-conjugated siRNAs) indicate dose-proportional pharmacokinetics and similar pharmacokinetics between chemical stabilizing methods.

Translation of clearance between species follows allometric principles.

Linear compartmental pharmacokinetic models with first-order absorption suffice to capture major trends in clinical pharmacokinetics of GalNAc-conjugated siRNAs.

Table 1 The considered GalNAc-siRNAs, their chemistry, and the species for which we retrieved plasma pharmacokinetics data in the literature

Compound	Chemistry	Rat	Monkey	Human
Revusiran	Alnylam's STC, triantennary GalNAc	O	O	O
Inclisiran	Alnylam's ESC, triantennary GalNAc	O	O	O
Vutrisiran	Alnylam's ESC, triantennary GalNAc	O	O	O
Givosiran	Alnylam's ESC, triantennary GalNAc	O	O	O
Lumasiran	Alnylam's ESC, triantennary GalNAc	O	O	O
Fitusiran	Alnylam's ESC, triantennary GalNAc			O
Olpasiran	Arrowhead's 21mers with blunt ends, triantennary GalNAc		O	O
Nedosiran	Dicerna's hairpin tetraloop, tetra-antennary GalNAc			O
SLN360	Silence's 19mers with blunt ends, triantennary GalNAc		O	O

Note that animal data could not be found for all compounds

GalNAc N-acetylgalactosamine *siRNAs* small-interfering ribonucleic acids, *STC* standard template chemistry, *ESC* enhanced stabilization chemistry

been examined in clinical trials and four of them, givosiran (acute hepatic porphyria), lumasiran (primary hyperoxaluria type 1), inclisiran (hypercholesterolemia), and vutrisiran (transthyretin-mediated amyloidosis) are currently approved by the US Food and Drug Administration (FDA) [2, 3]. The siRNA is composed of two nucleotide strands (each with a length of approximately 20 base-pairs), where the sequence of the antisense strand is designed to knockdown the expression of a target gene by mediating targeted mRNA degradation. To improve the efficacy, specificity, and stability of siRNAs, the natural structure of nucleotides is chemically modified at the phosphate backbone, the ribose moiety, and the base (see Hu et al. [4] for a comprehensive description).

Following subcutaneous administration, GalNAc-siRNAs rapidly distribute into the hepatocytes via asialoglycoprotein receptor (ASGPR)-mediated uptake followed by endocytosis. There is a continuous and sustained release of functionally active siRNAs from the endosomal depots into cytoplasm, where the siRNA elicits its pharmacodynamic effect [5]. The high stability of the siRNAs in the acidic environment of endosomes results in a long (10–100 days) biophase half-life [6, 7], which enables infrequent dosing. Typical clinical dosing frequencies of GalNAc-siRNAs range from once monthly to twice yearly [8], and the dose levels range from 25 to 300 mg per dosing occasion.

The plasma pharmacokinetics are characterized by an absorption phase over a period of a couple of hours, with maximum concentration typically achieved around 2–8 h post-dose, followed by a rapid distribution phase up to 24–48 h, in which the siRNA distributes mainly to the liver and kidney [9]. The last detectable concentration in plasma, above the lower limit of quantification of the bioanalytical assay, is often observed within 48 h [9]. Therefore, the detectable plasma concentrations are typically transient and not directly reflective of the long duration of action of siRNAs. However, albeit often not detectable, there is an extended linear elimination phase in plasma based on redistribution from tissue. This phase can last for months and reflects the long half-life of siRNAs in tissue.

Understanding how clinical pharmacokinetics relate to the dose and type of chemical stabilizing methods of the compounds is critical to interpret pharmacodynamic data, design animal and clinical studies, investigate safety windows, and to predict the human pharmacokinetics for new preclinical assets. McDougall et al. report that plasma pharmacokinetics in rats, monkeys and humans increase in a dose proportional manner at dose levels up to 10 mg/kg and greater than dose proportional at higher dose levels for a set of seven anonymized GalNAc-siRNAs from Alnylam Pharmaceuticals [9]. Furthermore, the same authors show that plasma pharmacokinetics are well correlated between species, suggesting that allometric scaling is feasible. However, there is currently no reported comprehensive analysis of clinical plasma pharmacokinetics across unambiguously defined GalNAc-siRNAs with different chemical stabilizing methods that have been in clinical testing, and there is no corresponding investigation of translation between animal and human for such compounds (c.f. [9, 10]).

Here, we close these gaps by presenting plasma pharmacokinetic data collected from the literature for nine GalNAc-siRNAs representing five different chemical stabilizing methods (Table 1). The main objective of our analysis was to show how the clinical plasma pharmacokinetics of GalNAc-siRNAs depend on dose level and type of siRNA chemical stabilizing method. By retrieving corresponding data from rats and monkeys, when available, we also investigate how the plasma pharmacokinetics of GalNAc-siRNAs differ and scale between species. As a secondary objective, we demonstrate and discuss what type of kinetic models are appropriate to describe the clinical plasma pharmacokinetic data retrieved.

2 Plasma Pharmacokinetics of N-Acetylgalactosamine (GalNAc)-Conjugated Small-Interfering Ribonucleic Acids (siRNAs)

2.1 Data Collection

Clinical pharmacokinetic parameters in the form of maximum concentration (C_{max}), area under the plasma drug concentration-time curve (AUC), and concentration-time data, if available, were collected from the literature for the following nine GalNAc-siRNAs: revusiran [11], inclisiran [12], vutrisiran [13], givosiran [14, 15], lumasiran [16, 17], fitusiran [18], olpasiran [19], nedosiran [20] and SLN360 [21]. The GalNAc-siRNA cemdisiran was excluded from the dataset because it is rapidly converted to a major active metabolite, AS(N-2)3′-cemdisiran, in healthy subjects [22]. Here, AUC generally refers to AUC$_\infty$. If AUC$_\infty$ was not reported, AUC$_{last}$ was used in our analysis. For GalNAc-siRNAs, this is an acceptable approximation when T_{last} is 24 or 48 h, since the terminal phase contributes little to the AUC. Reported values were the means/medians of 3–12 individuals. The dose level ranged from 5 to 900 mg, AUC ranged from 100 to 85,000 h*ng/mL, C_{max} ranged from 10 to 4000 ng/mL, and time to C_{max} (T_{max}) ranged from 1 to 12 h (mean 5 h, standard deviation [SD] 2.6 h). Data comprised heterogeneous populations (disease, ethnicity, sex) and different chemical stabilizing methods. The different bioanalytical methods used for the respective compounds are summarized in electronic supplementary material (ESM) Table S1.

Animal data on the plasma pharmacokinetics of GalNAc-conjugated siRNAs were collected for inclisiran [23], vutrisiran [24], givosiran [25], SLN360 [26], lumasiran [17], revusiran [27], and olpasiran [19]. Reported values were the means/medians of 3–8 individuals. The latter range is associated with uncertainty because the number of individuals was not reported for all studies. The dose level ranged from 0.1 to 300 mg/kg, AUC ranged from 70.1 to 1,920,000 h*ng/mL, C_{max} ranged from 11.2 to 90,900 ng/mL, and T_{max} ranged from 1 to 5.8 h (mean 2.4 h, SD 1.1 h). Data comprised heterogeneous populations (strain, sex) and different chemical stabilizing methods. All collected data are reported in a spreadsheet file in the ESM.

2.2 Model Regression

We used a linear model on a log-log scale to assess the relationship between dose/bodyweight and observed pharmacokinetic parameters (AUC/C_{max}) (Eqs. 1 and 2).

$$\log_{10} y = slope \log_{10} x + intercept, \tag{1}$$

alternatively expressed as

$$y = 10^{intercept} x^{slope}, \tag{2}$$

where y. is the dependent variable (e.g., AUC or C_{max}), x is the independent variable (e.g., dose or bodyweight), and *slope* and *intercept* are the estimated parameters. In the regression, each data point corresponds to the reported mean or median value per dose arm, and data were weighted by the number of subjects in the respective dose arm. Regression was performed by the function *fitlm* in MATLAB (R2019b; The MathWorks, Natick, MA, USA).

2.3 Human Plasma Pharmacokinetics

Our analysis indicates that the clinical plasma pharmacokinetics of GalNAc-conjugated siRNAs is approximately dose proportional and similar between the chemical stabilizing methods used (Fig. 1). This holds both for AUC and C_{max}. Data analysis confirmed a linear relationship (with slope ≈ 1) between the quantities on a $\log_{10} - \log_{10}$ scale, indicating approximately linear pharmacokinetics (Table 2). The conclusion holds both for dose in the form of milligrams (as shown in Fig. 1) and in the form of milligrams per kilogram of bodyweight (Fig. 2). The spread in the data is low and all parameters were well determined (Table 2).

2.4 Rat and Monkey Plasma Pharmacokinetics

Published rat and monkey data for plasma pharmacokinetics of GalNAc-conjugated siRNAs are sparse and we do not have the same coverage as for human data. Moreover, some of these data come from toxicology studies and are hence toxicokinetic data. For rats and monkeys, we retrieved data for five and seven of the nine GalNAc-siRNAs collected for humans (Table 1).

For rats, AUC increases supra-proportionally with dose (slope 1.38, and > 1 corresponding to dose-proportionality), while C_{max} is approximately dose proportional to dose (Fig. 3, upper panel; Table 2). Monkey data show the very same pattern, i.e. AUC increases supra-proportionally with dose (slope 1.34) and C_{max} is approximately dose proportional to dose (Fig. 3, lower panel; Table 2). The spread in data is low and all parameters were well determined (Table 2). Because the number of individuals was not reported for all studies, we repeated the regression without weighting and obtained very similar parameters (ESM Table S2).
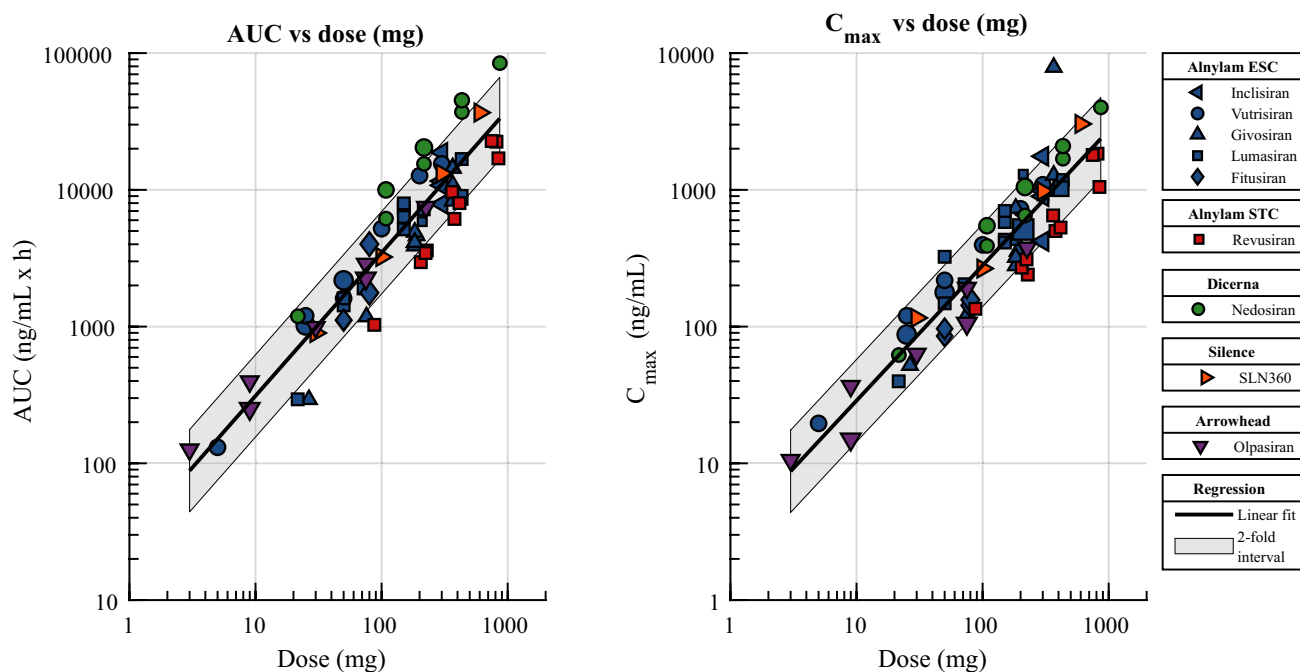
Fig. 1 Relationship between plasma AUC (left) and C_{max} (right) and dose, in milligrams, for GalNAc-conjugated siRNAs. The color indicates the type of chemistry, and the marker size reflects the number of subjects in the dose group. In each plot, the solid line represents the best linear fit and the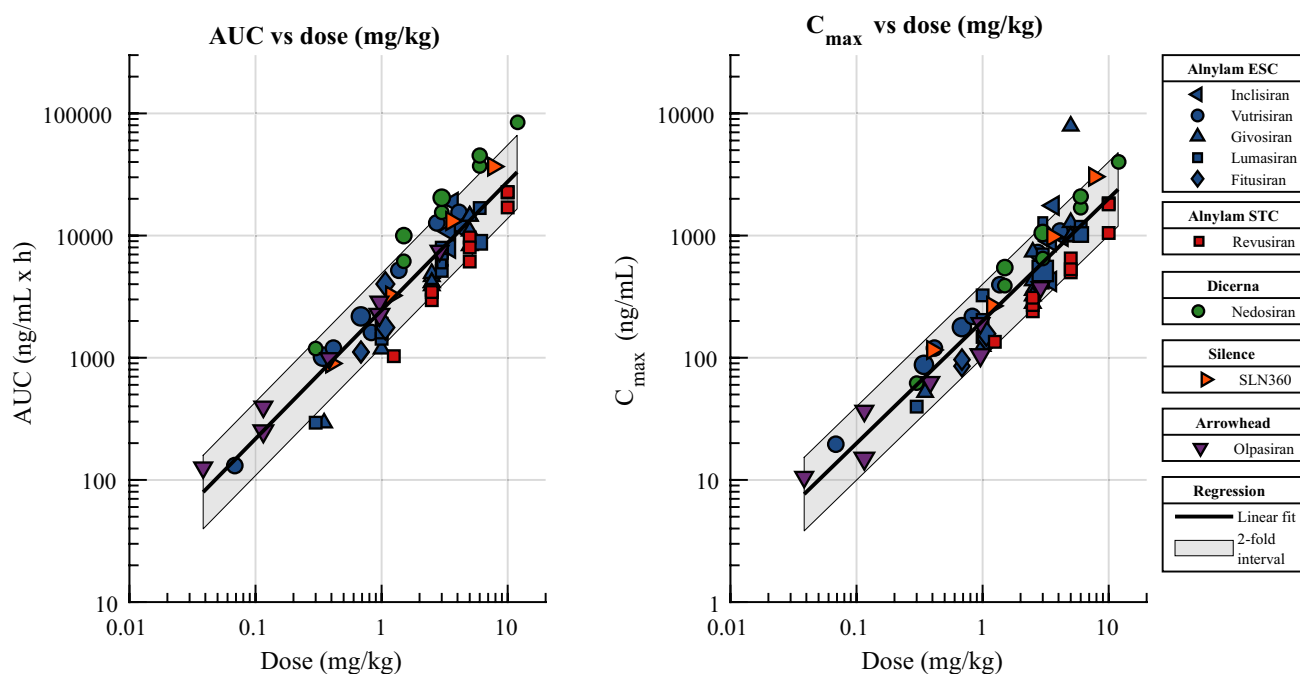 shaded area represents the twofold inter-val around the linear fit, covering most of the data points. *AUC* area under the concentration-time curve, C_{max} maximum concentration, *GalNAc* N-acetylgalactosamine, *siRNAs* small-interfering ribonu-cleic acids, *ESC* enhanced stabilization chemistry, *STC* standard tem-plate chemistry

Table 2 Parameter estimates of the linear model on a log-log scale

Regression	Species	Slope (SE)	Intercept (SE)	Figure
Dose (mg) vs. AUC	Human	1.05 (0.046)	1.45 (0.097)	1
Dose (mg) vs. C_{max}	Human	0.989 (0.046)	0.470 (0.097)	1
Dose (mg/kg) vs. AUC	Human	1.05 (0.046)	3.39 (0.026)	2
Dose (mg/kg) vs. C_{max}	Human	1.00 (0.043)	2.30 (0.024)	2
Dose (mg/kg) vs. AUC	Monkey	1.34 (0.022)	2.85 (0.030)	3
Dose (mg/kg) vs. C_{max}	Monkey	1.12 (0.019)	2.20 (0.026)	3
Dose (mg/kg) vs. AUC	Rat	1.38 (0.033)	2.26 (0.046)	3
Dose (mg/kg) vs. C_{max}	Rat	1.13 (0.046)	2.02 (0.062)	3
Body weight (kg) vs. CL/F (L/h)	Cross-species	0.751 (0.023)	0.064 (0.030)	4
Body weight (kg) vs. dose-normal-ized C_{max} (ng/mL / mg/kg)	Cross-species	0.0454 (0.016)	2.24 (0.021)	4

Equation 1 defines the slope and intercept parameters. The last column indicates which figure depicts the corresponding regression

SE standard error, *AUC* area under the concentration-time curve, C_{max} maximum concentration, *CL/F* apparent clearance

Fig. 2 Relationship between plasma AUC (left) and C_{max} (right) and dose, in milligrams per kilogram of bodyweight, for GalNAc-conjugated siRNAs. The color indicates the type of chemistry, and the marker size reflects the number of subjects in the dose group. In each plot, the solid line represents the best linear fit and the shaded area represents the twofold interval around the linear fit, covering most of the data points. *AUC* area under the concentration-time curve, C_{max} maximum concentration, *GalNAc* N-acetylgalactosamine, *siRNAs* small-interfering ribonucleic acids, *ESC* enhanced stabilization chemistry, *STC* standard template chemistry

## 2.5 Translation of Plasma Pharmacokinetics between Species

We then explored the translation of plasma pharmacokinetics of GalNAc-siRNAs between species, using the collected cross-species dataset. To this end, we applied allometric scaling using a power function to correlate physiological parameters with body size [31]. For clinical datasets without reported bodyweights, we applied a standard value of 70 kg for humans [32]. For preclinical datasets, we assumed standard bodyweights of 250 g for rats and 5 kg for monkeys [32]. Data indicate a slope of 0.75 for clearance over bioavailability (defined as CL/F = dose/AUC) [Fig. 4, Table 2]. The dose-normalized (on a milligrams/kilogram scale) C_{max} was constant with respect to bodyweight (Fig. 4, Table 2). For comparison, we also conducted the analysis for each compound individually (ESM Table S3), with similar overall results (the slope for clearance over bioavailability ranged from 0.60 to 0.86, with a median value of 0.75, and the slope for C_{max} was close to zero for all compounds).

3 Pharmacokinetic Models for GalNAc-Conjugated siRNAs

3.1 Empirical Models for Clinical Plasma Pharmacokinetics

There are several reported pharmacokinetic models of GalNAc-siRNAs [28]. On the empirical modeling side, the plasma pharmacokinetics of both givosiran and lumasiran were best described by two-compartment disposition models with first-order absorption when trained on data up to 48 h after dose [15, 29]. Similarly, we applied pharmacokinetic modeling using compartment models with first-order absorption and naïve-pooled analysis because of the lack of access to individual data. Modeling was done in Phoenix® WinNonlin® version 8.1.0.3530 (Certara USA, Inc., Princeton, NJ, USA).

Temporal clinical pharmacokinetic data in the form of mean plasma concentration over time were available for five of the GalNAc-siRNAs (inclisiran, givosiran, lumasiran, vutrisiran, and olpasiran) collected from the literature (Fig. 5). Data for olpasiran included time points up to 12 weeks after a single subcutaneous dose, while data for the other four compounds only included time points up to 24 or 48 h after dosing.
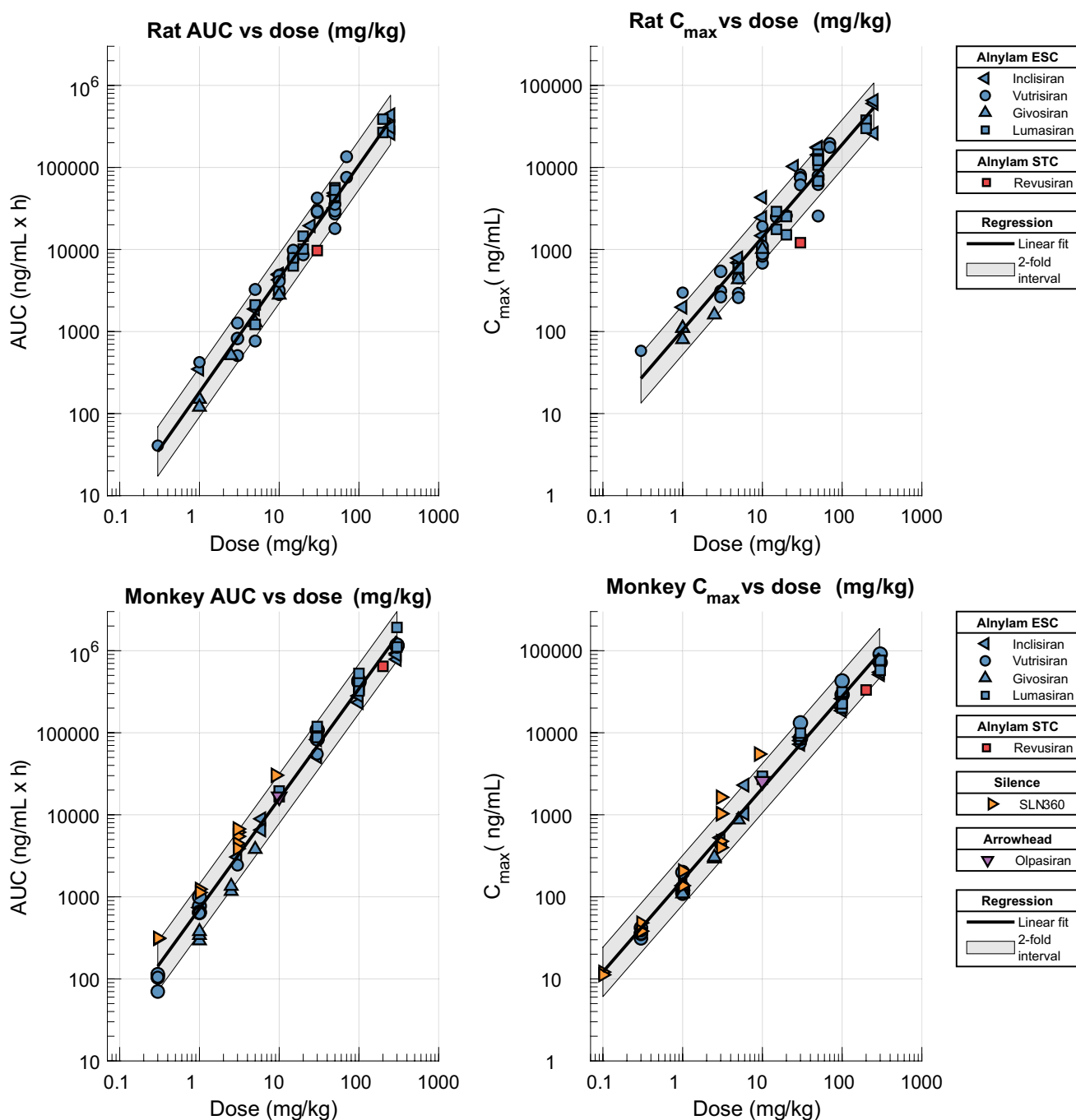
Fig. 3 Relationship between plasma AUC (left) and C_{max} (right) and dose, in milligrams per kilogram of bodyweight, for GalNAc-conjugated siRNAs in rats (upper panel) and monkeys (lower panel). The color indicates the type of chemistry, and the marker size reflects the number of subjects in the dose group. The number of subjects was assumed to be three if not reported. In each plot, the solid line represents the best linear fit and the shaded area represents the twofold interval around the linear fit, covering most of the data points. *AUC* area under the concentration-time curve, C_{max} maximum concentration, *GalNAc* N-acetylgalactosamine, *siRNAs* small-interfering ribonucleic acids, *ESC* enhanced stabilization chemistry, *STC* standard template chemistry

Plasma concentrations for the first 24 or 48 h after a single subcutaneous dose were well described by one-compartment kinetics with first-order absorption (ESM Table S4).

Plasma concentrations of olpasiran were best described by three-compartment kinetics (ESM Fig. S1; Table 3). Because of the similarity in pharmacokinetic properties between GalNAc-siRNAs (Figs. 1 and 2), the olpasiran
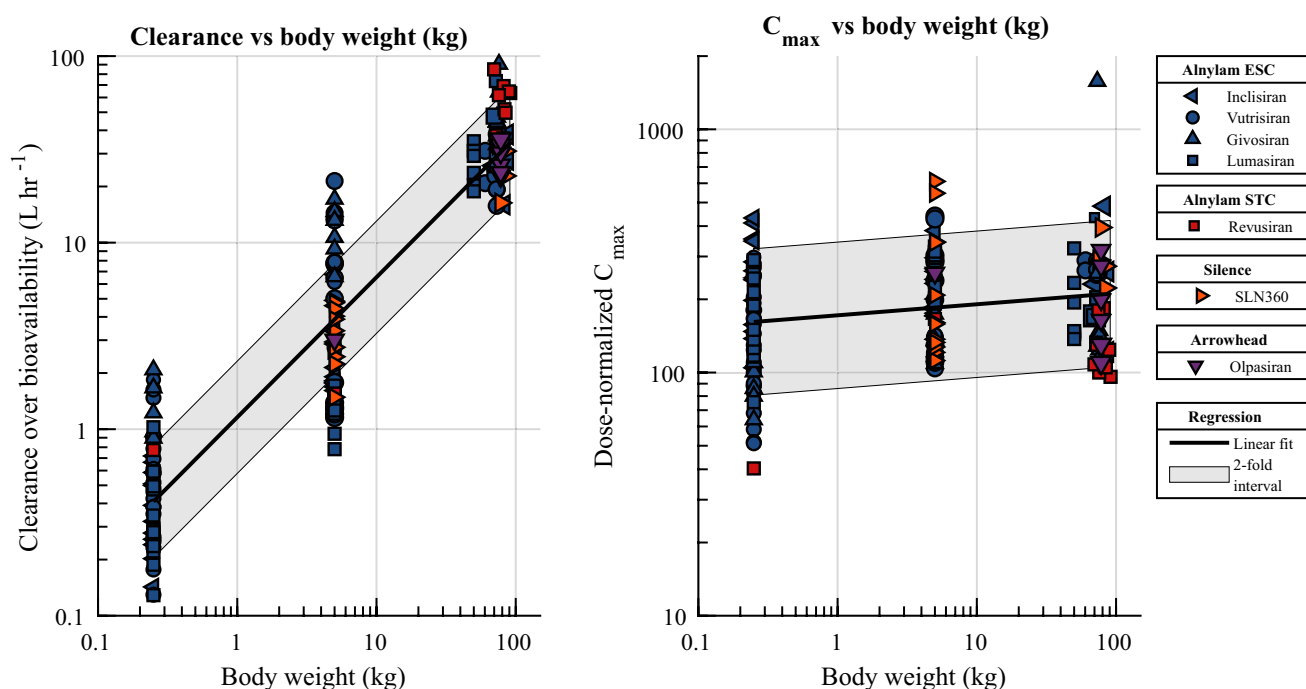
Fig. 4 Cross-species translation (rat, monkey, human) of plasma pharmacokinetics. *Left:* Clearance over bioavailability (CL/F = dose/AUC) versus body weight. *Right:* Dose-normalized C_{max} versus body weight. The color indicates the type of chemistry. In each plot, the solid line represents the best linear fit and the shaded area represents the twofold interval around the linear fit, covering most of the data points. *AUC* area under the concentration-time curve, C_{max} maximum concentration, *ESC* enhanced stabilization chemistry, *STC* standard template chemistry

three-compartment model with first-order absorption, based on the largest amount of data, was able to adequately predict exposures for the four other compounds (ESM Fig. S1). A three-compartment model, fitted jointly to data from all five compounds, provided similar and adequate predictions of plasma concentration, although model parameters differed from the olpasiran model (Fig. 5, Table 3).

3.2 A Physiologically Based Pharmacokinetic Model from the Literature

On the mechanistic modeling side, Ayyar et al. [30] have published a physiologically based pharmacokinetic (PBPK) model that was developed using published data for fitusiran and includes whole-body–to-cellular pharmacokinetic and pharmacodynamic properties. Specifically, the pharmacokinetics part includes hepatic biodistribution, GalNAc binding to ASGPRs on hepatocytes, ASGPR endocytosis and recycling, endosomal transport and escape of siRNAs, cytoplasmic RNA-induced silencing complex (RISC) loading, as well as pharmacodynamic degradation of target messenger RNA (mRNA) by bound RISC, and knockdown of protein. The model was implemented in the form of 14 ordinary differential equations and contains 48 parameters, of which 36 were obtained from the literature and the remaining 12

were estimated from data. The inputs are the dose level, dose route, and species (either mouse, rat, monkey or human), and the output is time courses of any of the model variables, e.g., drug concentration in plasma and liver, RISC-bound siRNA, and knockdown of the targeted mRNA or protein. Unfortunately, the reported equations do not generate the model simulations reported in the figures of the publication, and neither the model code nor the raw data are publicly available. We made six corrections to the published model equations to recreate, as faithfully as possible, the model simulations reported by Ayyar et al. [30]. We also compared model simulations with the olpasiran data, the only compound for which we retrieved time-course data over weeks, not only for the first 1 or 2 days. The corrected Ayyar model was implemented and simulated in MATLAB (R2019b; The MathWorks) and is available in the ESM.

The representative concentration-time course data for olpasiran were compared with simulations of the PBPK model by Ayyar et al. [30]. The PBPK model predicted olpasiran plasma pharmacokinetics relatively well in the time interval for which the model was trained, i.e., for the first days after dose, but failed to extrapolate beyond 168 h (Fig. 6).
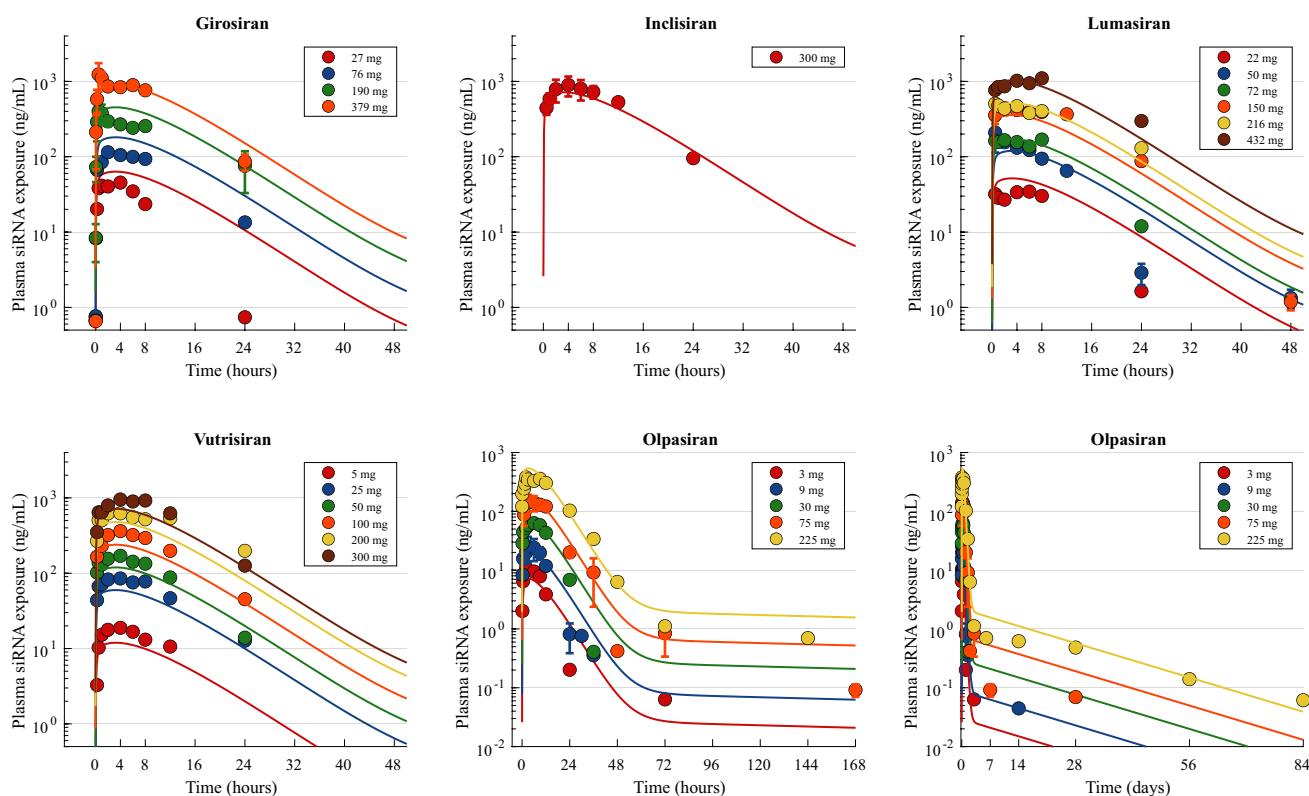
Fig. 5 Reported plasma concentration-time data (circles) of the Gal-NAc-siRNAs inclisiran, givosiran, lumasiran, vutrisiran, and olpasiran. For the four first of these GalNAc-siRNAs, data were collected for 24 or 48 h after a single subcutaneous dose. For olpasiran, data were collected over 84 days after a single subcutaneous dose; the first olpasiran panel shows the first week after dosing, and the second olpasiran panel shows the full 84-day time course with detect-able concentrations for the high dose of 225 mg up to the very last observation point. For cases with reported data for several patient populations on the same dose level, the mean and SEM is plotted. The solid lines represent simulations of the linear three-compartment pharmacokinetic model fitted jointly to data from all five compounds. *GalNAc* N-acetylgalactosamine, *siRNAs* small-interfering ribonucleic acids, *SEM* standard error of the mean

4 Discussion and Conclusions

4.1 Plasma Pharmacokinetics of GalNAc-Conjugated siRNAs

We collected and analyzed literature pharmacokinetic data for nine GalNAc-conjugated siRNAs. Based on this analysis, we showed that the clinical plasma AUC and C_{max} of Gal-NAc-conjugated siRNAs are approximately dose propor-tional and similar between the chemical stabilizing meth-ods used. The reported linear regression equations for AUC and C_{max}, in combination with the approximately twofold uncertainty, can be useful to predict and reason about plasma pharmacokinetics for other GalNAc-conjugated siRNAs.

To support the design and interpretation of animal studies and to reason about translation, we collected cor-responding plasma pharmacokinetics and toxicokinetic data from rodents and monkeys. Like human data, animal data indicate dose-proportional C_{max} and similar kinetics between compounds with different chemical stabilizing methods. However, in contrast to human data, animal data

Table 3 Parameters of the linear three-compartment pharmacoki-netic model with first-order absorption fitted to olpasiran data only, and simultaneously fitted to data for inclisiran, givosiran, lumasiran, vutrisiran, and olpasiran

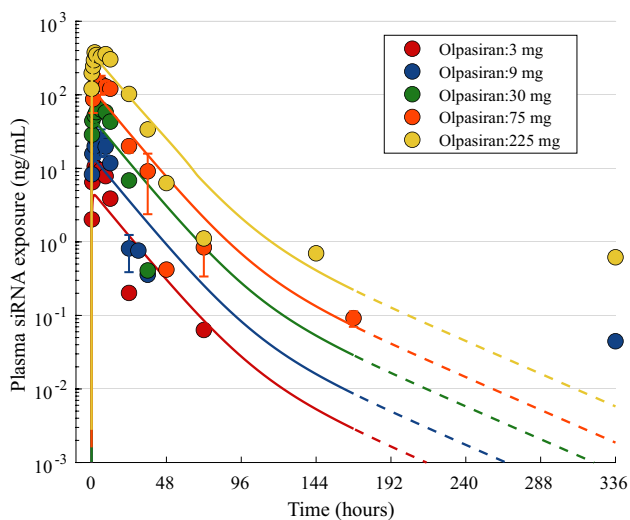| Parameter	Model fitted to olpasiran data only [estimate (SE)]	Model simultaneously fitted to all data [estimate (SE)]
Ka (1/h)	0.635 (0.21)	0.157 (0.031)
V1/F (L)	27.9 (5.6)	18.1 (4.1)
V2/F (L)	1470 (370)	1340 (180)
V3/F (L)	296 (39)	100 (30)
CL1/F (L/h)	27.7 (2.4)	23.8 (0.77)
CL2/F (L/h)	2.62 (1.4)	3.02 (0.37)
CL3/F (L/h)	914 (560)	45.4 (15)

Each parameter is reported by the point estimates followed by the estimated SE in parentheses. The estimated V and CL parameters are reported as ratios of the F, because only extravascular data are avail-able and it is impossible to estimate true clearances and volumes

SE standard error, *V* volume, *CL* clearance, *F* bioavailability

Fig. 6 Comparison of Ayyar's PBPK model simulations (lines) with plasma concentration-time course data (circles) of the representative GalNAc-siRNA olpasiran. The dotted lines represent extrapolation outside the range of the training data set. For cases with reported data for several patient populations on the same dose level, the mean and standard error of the mean is plotted. *GalNAc* N-acetylgalactosamine, *siRNA* small-interfering RNA

show supra-dose-proportional AUCs. Our observation that plasma AUC is approximately dose proportional in humans at therapeutic dose levels, and greater than dose proportional in monkeys for a wider dose range up to 300 mg/kg, agrees with data reported by McDougall et al. [9] for seven GalNAc-siRNAs with unknown targets and sequences. The supra-proportionality observed when including higher dose levels is likely due to transient saturation of the ASGPR, which takes up the GalNAc-siRNA to the hepatocytes [9]. The dose ranges differ between animals and humans because the animal studies contain data from toxicity studies at dose levels up to 300 mg/kg. It is likely that human data would also show supra-proportionality if studied at greater than therapeutic dose levels. We note that awareness of potential non-linearities in pharmacokinetics is critical to correctly interpret how high-dose levels impact pharmacodynamics.

Translation between species follows allometric principles with a clearance over bioavailability exponent of 0.75. The estimate is based on an analysis of all data simultaneously, but a similar result is obtained when each compound is analyzed individually. The value aligns well to the often-assumed slope of 0.75, sometimes referred to as Kleiber's law [33], which also has empirical support for various drug classes, including oligonucleotides, e.g., Jansen et al., Oitate et al., and Geary et al. [34–36].

Although plasma pharmacokinetics are similar for various GalNAc-siRNAs, the target tissue half-life may differ substantially (1.5–14 weeks in humans) [6]. Therefore, the dose level and dosing frequency of *in vivo* efficacy studies

are mainly determined by biomarker response data over weeks, and not by plasma pharmacokinetic data sampled over only 24–48 h. Nevertheless, plasma pharmacokinetics are critical for reasoning on safety windows and on how non-linearities in pharmacokinetics may affect pharmacodynamics. Moreover, plasma pharmacokinetics observed over weeks, requiring high-sensitivity bioanalysis methods, would likely be useful for both efficacy and safety reasoning.

4.2 Pharmacokinetic Models for GalNAc-Conjugated siRNAs

Clinical plasma concentration-time profiles of GalNAc-siRNAs can be described by one-compartment kinetics with first-order absorption over the first 24 h, and by three-compartment kinetics for the rare case when additional later time-points up to several weeks after dosing were sampled and exposure detected. The reported models can be useful in the preclinical phase of new GalNAc-siRNAs, e.g., to reason about safety windows. When the first pharmacokinetic data have been generated in phase I, it is natural to develop a clinical pharmacokinetic model specifically to the GalNAc-siRNAs under consideration. The three-compartment models, based on data from either olpasiran alone or five GalNAc siRNAs, differ noticeably in several model parameters, including absorption rate (K_a). This is somewhat in agreement with the estimated range of K_a values for the one-compartment models (ESM Table S4) and should also be viewed in relation to the moderately large standard errors for the parameters in the olpasiran model. In contrast, the model based on all data features much smaller standard errors for all parameters and appears more robust. However, some caution is warranted to avoid overinterpreting, specifically those parameters in which the two models differ.

An alternative to compartmental models is to develop a mechanistic model allowing a broader range of scenarios to be tested, e.g., simulations of tissue pharmacokinetics and GalNAc uptake. We exemplify this type of model using the reported PBPK model by Ayyar et al. [30]. The usefulness of this model is limited by two factors. First, the model code and raw data are not included in the publication, and the reported equations and parameters fail to reproduce the simulations in the published paper. Second, the model is not trained on plasma pharmacokinetic data beyond 48 h and fails to describe such data for olpasiran. By identifying and correcting several errors in the published model equations, we managed to recreate, as faithfully as possible, the model simulations reported by Ayyar et al. [30]. Despite its limitations, we believe the PBPK model can be a good starting point for improved mechanistic models of the pharmacokinetics of GalNAc-siRNAs, and we report our corrected model to facilitate such extensions (see the ESM).

Today, when reasoning about the clinical plasma pharmacokinetics in the preclinical phase of a new GalNAc-siRNA, we argue that our proposed three-compartment models (Table 3) constitute good model choices when simulations over weeks are desired. In comparison with the reported PBPK model, they more accurately describe the terminal plasma half-life. For simulations over 24–48 h, any of the reported simpler one-compartment models are adequate.

In general, both simple (e.g., allometric and compartmental) and complex (e.g., PBPK) models have their advantages and disadvantages. Briefly, the relevant model complexity depends on (1) data quality and quantity; (2) prior information of the system; and (3) the research question to be addressed. Because of this, it is common and natural that several models, defined at different levels of complexity, exist in parallel. Models of the type presented here can help to address several research questions in the discovery phase. Overall, they can support decision making all the way from target selection to candidate selection. Specifically, they can inform the choice of type of drug class (e.g., small molecule, peptide, or siRNA) that is adequate from an efficacy and safety perspective to hit a certain target, they can help to guide the design of in vivo experiments, and anchoring reasoning about the translational aspects of a new candidate compound, from both a pharmacokinetic/pharmacodynamic perspective and a toxicokinetic-to-safety perspective. In this context, the benefits of a simple model, compared with a complex PBPK model, include simple to implement, simple to use, and simple to unambiguously define. The benefits of a PBPK model include mechanistic insight, e.g., considering species differences of both receptor density and the receptor turnover rate of ASGPR, and the much wider range of possible simulations. Naturally, the value of a certain model, independently of model complexity, increases if it has been shown that the pharmacokinetics of the drug class are similar between different chemical modifications, something that we have shown here for GalNAc-siRNAs.

4.3 Limitations of the Analysis

We have identified the following main limitations of our analysis. First, the number of investigated GalNAc-siRNAs is limited; nine for humans, seven for monkeys, and five for rats. This reflects the relatively low number of GalNAc-siRNAs with clinical pharmacokinetic data in the public domain, although the numbers are expected to gradually increase in the coming years. On the other hand, there is relatively low spread in our AUC and C_{max} regressions, with approximately twofold uncertainty around the point predictions. Second, our analysis uses mean or median data and not individual data; therefore, any prediction using our models should be interpreted on the group level and not on the individual level. Third, the group size for the animal studies was not always reported and an assumption of three subjects per group was made when the information was missing. However, similar parameters were obtained when repeating the regression without weighting (see the ESM), indicating that the sensitivity to this assumption is at least not severe. Fourth, the rat analysis was performed on compounds only representing Alnylam's chemical stabilizing method. However, our data indicate no dependency between plasma pharmacokinetics and the chemical stabilizing method in monkeys and humans, and it is therefore likely that the same holds in rats. Fifth, one cannot exclude some variability in accuracy and precision between the various bioanalytical methods used for the different compounds (ESM Table S1).

5 Conclusions

We have presented the first comprehensive analysis of the clinical plasma pharmacokinetics of GalNAc-siRNAs, including pharmacokinetic modeling aspects, as well as a corresponding analysis of animal plasma pharmacokinetics, including cross-species translation. We believe these results can help to interpret pharmacodynamic data, design animal and clinical studies, define safety windows, and to predict the pharmacokinetics for new preclinical assets across species.

References

1. Ranasinghe P, Addison ML, Dear JW, Webb DJ. Small interfering RNA: Discovery, pharmacology and clinical development-An introductory review. Br J Pharmacol. 2022. https://doi.org/10.1111/bph.15972.

2. Friedrich M, Aigner A. Therapeutic siRNA: State-of-the-Art and future perspectives. BioDrugs. 2022;36(5):549–71.

3. Jing X, Arya V, Reynolds KS, Rogers H. Clinical pharmacology of RNA interference-based therapeutics: a summary based on food and drug administration-approved small interfering RNAs. Drug Metab Dispos. 2023;51(2):193–8.

4. Hu B, Zhong L, Weng Y, Peng L, Huang Y, Zhao Y, et al. Therapeutic siRNA: state of the art. Signal Transduct Target Ther. 2020;5(1):101.

5. Dowdy SF, Setten RL, Cui XS, Jadhav SG. Delivery of RNA therapeutics: The Great Endosomal Escape! Nucleic Acid Ther. 2022;32(5):361–8.

6. Boianelli A, Aoki Y, Ivanov M, Dahlen A, Gennemark P. Cross-species translation of biophase half-life and potency of GalNAc-conjugated siRNAs. Nucleic Acid Ther. 2022;32(6):507–12.

7. Brown CR, Gupta S, Qin J, Racie T, He G, et al. Investigating the pharmacodynamic durability of GalNAc-siRNA conjugates. Nucleic Acids Res. 2020;48(21):11827–44.

8. Zhang MM, Bahal R, Rasmussen TP, Manautou JE, Zhong XB. The growth of siRNA-based therapeutics: updated clinical studies. Biochem Pharmacol. 2021;189:114432.

9. McDougall R, Ramsden D, Agarwal S, Agarwal S, Aluri K, et al. The nonclinical disposition and pharmacokinetic/pharmacodynamic properties of N-acetylgalactosamine-conjugated small interfering RNA are highly predictable and build confidence in translation to human. Drug Metab Dispos. 2022;50(6):781–97.

10. Humphreys SC, Davis JA, Iqbal S, Kamel A, Kulmatycki K, et al. Considerations and recommendations for assessment of plasma protein binding and drug-drug interactions for siRNA therapeutics. Nucleic Acids Res. 2022;50(11):6020–37.

11. Zimmermann TS, Karsten V, Chan A, Chiesa J, Boyce M, et al. Clinical proof of concept for a novel hepatocyte-targeting GalNAc-siRNA conjugate. Mol Ther. 2017;25(1):71–8.

12. Wright RS, Collins MG, Stoekenbroek RM, Robson R, Wijngaard PLJ, et al. Effects of renal impairment on the pharmacokinetics, efficacy, and safety of inclisiran: an analysis of the ORION-7 and ORION-1 studies. Mayo Clin Proc. 2020;95(1):77–89.

13. Habtemariam BA, Karsten V, Attarwala H, Goel V, Melch M, et al. Single-dose pharmacokinetics and pharmacodynamics of transthyretin targeting N-acetylgalactosamine-small interfering ribonucleic acid conjugate, vutrisiran, healthy subjects. Clin Pharmacol Ther. 2021;109(2):372–82.

14. Agarwal S, Simon AR, Goel V, Habtemariam BA, Clausen VA, Kim JB, Robbie GJ. Pharmacokinetics and pharmacodynamics of the small interfering ribonucleic acid, givosiran, in patients with acute hepatic porphyria. Clin Pharmacol Ther. 2020;108(1):63–72.

15. US FDA. New Drug Application (NDA 212194), Multi-disciplinary Review and Evaluation, GIVLAARI (givosiran). 2018 [cited 23 Mar 2023]. https://www.accessdata.fda.gov/drugsatfda_docs/nda/2019/212194Orig1s000MultidisciplineR.pdf.

16. Frishberg Y, Deschenes G, Groothoff JW, Hulton SA, Magen D, et al. Phase 1/2 Study of Lumasiran for Treatment of Primary Hyperoxaluria Type 1: A Placebo-Controlled Randomized Clinical Trial. Clin J Am Soc Nephrol. 2021;16(7):1025–36.

17. European Medicines Agency (EMA). Assessment report Oxlumo, EMA/568312/2020. 2020 [cited 24 Mar 2023]. https://www.ema.europa.eu/en/documents/assessment-report/oxlumo-epar-public-assessment-report_en.pdf.

18. Pasi KJ, Lissitchkov T, Mamonov V, Mant T, Timofeeva M, et al. Targeting of antithrombin in hemophilia A or B with investigational siRNA therapeutic fitusiran-Results of the phase 1 inhibitor cohort. J Thromb Haemost. 2021;19(6):1436–46.

19. Koren MJ, Moriarty PM, Baum SJ, Neutel J, Hernandez-Illas M, et al. Preclinical development and phase 1 trial of a novel siRNA targeting lipoprotein(a). Nat Med. 2022;1:96–103.

20. Hoppe B, Koch A, Cochat P, Garrelfs SF, Baum MA, et al. Safety, pharmacodynamics, and exposure-response modeling results from a first-in-human phase 1 study of nedosiran (PHYOX1) in primary hyperoxaluria. Kidney Int. 2022;101(3):626–34.

21. Nissen SE, Wolski K, Balog C, Swerdlow DI, Scrimgeour AC, et al. Single ascending dose study of a short interfering RNA targeting lipoprotein(a) production in individuals with elevated plasma lipoprotein(a) levels. JAMA. 2023;327(17):1679–87.

22. Badri P, Jiang X, Borodovsky A, Najafian N, Kim J, Clausen VA, et al. Pharmacokinetic and pharmacodynamic properties of cemdisiran, an RNAi therapeutic targeting complement component 5, in healthy subjects and patients with paroxysmal nocturnal hemoglobinuria. Clin Pharmacokinet. 2021;60(3):365–78.

23. US FDA. Non-clinical review Inclisiran, Application number: 214012Orig1s000. 2019 [cited 24 Mar 2023]. https://www.accessdata.fda.gov/drugsatfda_docs/nda/2022/214012Orig1s000PharmR.pdf.

24. US FDA. Non-clinical review AMVUTTRA® (vutrisiran), Application number: 215515Orig1s000. 2022 [cited 24 Mar 2023]. https://www.accessdata.fda.gov/drugsatfda_docs/nda/2022/215515Orig1s000PharmR.pdf.

25. European Medicines Agency (EMA). Assessment report Givlaari, EMA/CHMP/70703/2020. 2020 [cited 24 Mar 2023]. https://www.ema.europa.eu/en/documents/assessment-report/givlaari-epar-public-assessment-report_en.pdf.

26. Rider DA, Eisermann M, Loffler K, Aleku M, Swerdlow DI, et al. Pre-clinical assessment of SLN360, a novel siRNA targeting LPA, developed to address elevated lipoprotein (a) in cardiovascular disease. Atherosclerosis. 2022;349:240–7.

27. Sutherland JE, Hettinger JL, Chan A, Gilbert J, Warner GL, Davis WP. Nonclinical safety profile of revusiran, a 1st-generation GalNAc-siRNA conjugate for treatment of hereditary transthyretin-mediated amyloidosis. Nucleic Acid Ther. 2020;30(1):33–49.

28. Jeon JY, Ayyar VS, Mitra A. Pharmacokinetic and pharmacodynamic modeling of siRNA therapeutics—a Minireview. Pharm Res. 2002;39(8):1749–59.

29. US FDA. New Drug Application (NDA 214103), Integrated Review, Oxlumo (Lumasiran). 2020 [cited 28 Mar 2023]. https://www.accessdata.fda.gov/drugsatfda_docs/nda/2020/214103Orig1s000IntegratedR.pdf.

30. Ayyar VS, Song D, Zheng S, Carpenter T, Heald DL. Minimal physiologically based pharmacokinetic-pharmacodynamic (mPBPK-PD) model of N-acetylgalactosamine-conjugated small interfering RNA disposition and gene silencing in preclinical species and humans. J Pharmacol Exp Ther. 2021;379(2):134–46.

31 Huh Y, Smith DE, Feng MR. Interspecies scaling and prediction of human clearance: comparison of small- and macro-molecule drugs. Xenobiotica. 2011;41(11):972–87.

32 Davies B, Morris T. Physiological parameters in laboratory animals and humans. Pharm Res. 1993;10(7):1093–5.

33. Kleiber M. Body size and metabolic rate. Physiol Rev. 1947;27(4):511–41.

34 Jansen K, PouCasellas C, Groenink L, Wever KE, Masereeuw R. Humans are animals, but are animals human enough? A systematic review and meta-analysis on interspecies differences in renal drug clearance. Drug Discov Today. 2020;25(4):706–17.

35. Oitate M, Masubuchi N, Ito T, Yabe Y, Karibe T, et al. Prediction of human pharmacokinetics of therapeutic monoclonal antibodies from simple allometry of monkey data. Drug Metab Pharmacokinet. 2011;26(4):423–30.

36. Geary RS, Yu RZ, Watanabe T, Henry SP, Hardee GE, et al. Pharmacokinetics of a tumor necrosis factor-alpha phosphorothioate 2'-O-(2-methoxyethyl) modified antisense oligonucleotide: comparison across species. Drug Metab Dispos. 2003;31(11):1419–28.